Inorg. Chem. **2007**, *46*, 9630–9640

Syntheses, Structures, and Properties of Five Coordination Polymers Containing Fluorescent Whitener

Ruibiao Fu, Shengmin Hu, and Xintao Wu*

State Key Laboratory of Structural Chemistry, Fujian Institute of Research on the Structure of Matter, Chinese Academy of Science, Fuzhou, Fujian, 350002 China

Received March 29, 2007

Fluorescent whitener (4,4′-bis(2-sulfonatostiryl)biphenyl) was incorporated with M/4,4′-bipy (M = Cd, Co; 4,4′-bipy=4,4′-bipyridine) 2D frameworks, Mn/4,4′-bipyH fragment, and the $[Zn_2(Im)_2(ImH)_4]^{2+}$ (ImH = imidazole) chain under hydrothermal conditions to obtain seven new coordination polymers: $[Cd(4,4'\text{-bipy})(L)(H_2O)_2]$ (**1**), $[Co(4,4'\text{-bipy})_2(L)]\cdot 2H_2O$ (**2**), $[Co(4,4'\text{-bipy})_2(H_2O)_2](4,4'\text{-bipy})(L)\cdot 2H_2O$ (**3**), $[Mn(4,4'\text{-bipyH})_2(L)_2(H_2O)_2]\cdot 4H_2O$ (**4**), and $[Zn_2(Im)_2(ImH)_4](L)$ (**5**). Their structures were determined by single-crystal X-ray diffraction. In **1**, binuclear $[Cd_2]$ units are bridged by 4,4′-bipys into a 2D cationic framework, which is further penetrated by **L** anions. **2** has an organic–inorganic hybrid layer consisting of $[Co(4,4'\text{-bipy})_2]$ squarelike motifs and **L** anions. **3** features a pcu-like 3D cationic framework with the inclusion of **L** anions. In **4**, the $[Mn(4,4'\text{-bipyH})_2(H_2O)_2]^{4+}$ cationic fragment is sandwiched by **L** anions into a sandwichlike hybrid layer. **5** exhibits a 3D honeycomb-like structure with each nanotube encapsulating two parallel **L** anionic chains. TGA and PXRD indicate solids **1**, **4**, and **5** are thermally stable up to 280, 200, and 250 °C under an air atmosphere, respectively. **1** has bright blue-green luminescence with a peak maximum band at about 470 nm. **4** exhibits tunable emission between dark-red and weak-green under the excitation of 500 and 280 nm, respectively. **5** displays a bright blue-green emission with a peak band at 454 nm and a shoulder peak at 473 nm. It is attractive that the luminescent properties of solids **1**, **4**, and **5** are almost retained after heat treatment at 200, 200, and 250 °C for 2 h under an air atmosphere, respectively.

Introduction

The design and synthesis of coordination polymers based on metal-organic frameworks (MOFs) is of great research interest during the past decade, owing to their structural diversities and intriguing properties, including gas adsorption, enantioselective separation, catalysis, electrical conductivity, nonlinear optics, and so on.[1] In particular, the synthesis of luminescent coordination polymers has flourished because of their potential applications as light-emitting diodes, chemosensors, probes, and sensors.[2−5] One very important reason is that most luminescent coordination polymers exhibit higher thermal stability and stronger intensity than those of free organic ligands.[1a,2h,4d] Another reason is that luminescent colors can be tuned through judicious choices of organic bridging ligands and metal nodes, like the bathochromic-shift and the blue-shift.[2] In this regard, an effective strategy to obtain bright luminescent solids is the combination of the fluorescent organic unit with MOFs via electrostatic interac-

* To whom correspondence should be addressed. E-mail: wxt@fjirsm.ac.cn.

(1) (a) Janiak, C. *Dalton Trans.* **2003**, 2781−2804. (b) Rosi, N. L.; Kim, J.; Eddaoudi, M.; Chen, B.; O'Keeffe, M.; Yaghi, O. M. *J. Am. Chem. Soc.* **2005**, *127*, 1504−1518. (c) Yaghi, O. M.; Li, G.; Li, H. *Nature* **1995**, *378*, 703−706. (d) Kesanli, B.; Cui, Y.; Smith, M. R.; Bittner, E. W.; Bockrath, B. C.; Lin, W. *Angew. Chem., Int. Ed.* **2005**, *44*, 72−75. (e) Seo, J. S.; Whang, D.; Lee, H.; Jun, S. I.; Oh, J.; Jeon, Y. J.; Kim, K. *Nature* **2000**, *404*, 982−986. (f) Fujita, M.; Kwon, Y. J.; Washizu, S.; Ogura, K. *J. Am. Chem. Soc.* **1994**, *116*, 1151−1152. (g) Zheng, S. L.; Zhang, J. P.; Wong, W. T.; Chen, X. M. *J. Am. Chem. Soc.* **2003**, *125*, 6882−6883. (h) Evans, O. R.; Lin, W. *Acc. Chem. Res.* **2002**, *35*, 511−522.

(2) (a) Dong, Y. B.; Jin, G. X.; Smith, M. D.; Huang, R. Q.; Tang, B.; zur Loye, H. C. *Inorg. Chem.* **2002**, *41*, 4909−4914. (b) Zheng, S. L.; Tong, M. L.; Tan, S. D.; Wang, Y.; Shi, J. X.; Tong, Y. X.; Lee, H. K.; Chen, X. M. *Organometallics* **2001**, *20*, 5319−5325. (c) Chen, Z. F.; Xiong, R. G.; Zhang, J.; Zuo, J. L.; You, X. Z.; Che, C. M.; Fun, H. K. *J. Chem. Soc., Dalton Trans.* **2000**, 4010−4012. (d) Guo, X. D.; Zhu, G. S.; Fang, Q. R.; Xue, M.; Tian, G.; Sun, J. Y.; Li, X. T.; Qiu, S. L. *Inorg. Chem.* **2005**, *44*, 38500−3855. (e) Dai, J. C.; Wu, X. T.; Fu, Z. Y.; Cui, C. P.; Hu, S. M.; Du, W. X.; Wu, L. M.; Zhang, H. H.; Sun, R. Q. *Inorg. Chem.* **2002**, *41*, 1391−1396. (f) Fu, R. B.; Xiang, S. C.; Hu, S. M.; Wang, L. S.; Li, Y. M.; Huang, X. H.; Wu, X. T. *Chem. Commun.* **2005**, 5292−5294. (g) Dai, J. C.; Wu, X. T.; Hu, S. M.; Fu, Z. Y.; Zhang, J. J.; Du, W. X.; Zhang, H. H.; Sun, R. Q. *Eur. J. Inorg. Chem.* **2004**, 2096−2106. (h) Paul, B.; Zimmermann, B.; Fromm, K. M.; Janiak, C. *Z. Anorg. Allg. Chem.* **2004**, *630*, 1650−1654.

10.1021/ic700597k CCC: $37.00
Published on Web 09/28/2007

tion, covalent bonds, hydrogen bonds, and $\pi-\pi$ stacking interactions. Following this strategy, fluorescent whiteners would be introduced as building blocks into MOFs because they can absorb UV radiation and emit bright-blue visible light. 4,4′-Bis(2-sulfonatostiryl)biphenyl (denoted as **L**), which is a stilbene-type fluorescent whitener with an luminescent quantum yield of 0.8, has been successfully assembled with the zinc/4,4′-bipy cationic framework into a bright-green luminescent solid.[2f,6] The zinc solid exhibits a ~90 nm bathochromic-shift compared to that of **Na_2L** and possesses a very broad excitation spectrum. To expand our research, we have altered metal centers, ratios of reactants, and organic bridging ligands to obtain other coordination polymers with fascinating structures and luminescent properties. In this article, we report the syntheses, crystal structures, and properties of five new coordination polymers containing fluorescent whitener, namely, [Cd(4,4′-bipy)(L)(H_2O)$_2$] (**1**), [Co(4,4′-bipy)$_2$(L)]·2H_2O (**2**), [Co(4,4′-bipy)$_2$(H_2O)$_2$](4,4′-bipy)(L)·2H_2O (**3**), [Mn(4,4′-bipyH)$_2$(L)$_2$(H_2O)$_2$]·4H_2O (**4**), and [Zn_2(Im)$_2$(ImH)$_4$] (L) (**5**).

Experimental Section

Materials and Methods. All of the chemicals were obtained from commercial sources without further purification. **1**−**5** were synthesized in 25 mL Teflon-lined stainless steel vessels under autogenous pressure. The reactants were stirred homogeneously before heating. Elemental analyses were carried out with a Vario EL III element analyzer. Infrared spectra were obtained on a Nicolet Magna 750 FTIR spectrometer. The diffuse reflectance spectrum of **2** was recorded on a PerkinElmer Lambda 35 UV−vis spectrometer. Photoluminescence analyses for solids **1**−**2**, **4**, and **5** were performed with an Edinburgh FLS920 and LifeSpec-ps fluorescence spectrometers. Thermogravimetric analysis (TGA) was performed on a NETZSCH STA449C under nitrogen gas flow at a heating rate of 15 °C·min^{-1} from room temperature to 800 °C. Powder X-ray diffraction (XRD) patterns were acquired on a DMAX-2500 diffractometer using Cu Kα radiation in the ambient environment. Magnetic measurements for **2** were carried out with a Quantum Design PPMS model 6000 magnetometer at 5 KOe in the temperature range of 2−308 K.

Syntheses of [Cd(4,4′-bipy)(L)(H_2O)$_2$] (1). A mixture of Cd(CH_3COO)$_2$·2H_2O(0.0256 g, 0.0960 mmol), Na_2L(0.0565 g, 0.1004 mmol), 4,4′-bipyridine (0.0185 g, 0.1184 mmol), and H_2O (10.0 mL, 556 mmol) was heated at 140 °C for 168 h. After the mixture was cooled slowly to ambient temperature, light-orange prism-shaped crystals were obtained. The final pH of the solution was 4.82. The crystals were filtered, washed with distilled water, and dried at ambient temperature. A suitable crystal was selected for single-crystal X-ray diffraction studies. The pattern of experimental powder XRD was in accord with those simulated from single-crystal X-ray data, which indicated the homogeneous phase of the product. The yield was about 43% (0.0341 g) based on Cd(CH_3COO)$_2$·2H_2O. Anal. Calcd for $C_{38}H_{32}N_2O_8S_2Cd$ **1**: C 55.58, H 3.93, N 3.41. Found: C 55.63, H 4.01, N 3.58. IR (KBr pellet, cm^{-1}): 3450m(ν_{O-H}), 3346m(ν_{O-H}), 3049(ν_{C-H}), 3030w($\nu_{C=C-H}$), 3005w ($\nu_{C=C-H}$), 1610m ($\nu_{C=C}$), 1568w, 1539m, 1495m, 1464m, 1417m, 1329w, 1228vs, 1171vs, 1134s, 1078m, 1041m, 1014s, 968w, 960m, 945w, 880w, 856w, 818w, 806m, 775m, 762m, 742w, 723w, 698w, 975w, 631m, 611m, 594m, 569m, 536m, 457w. In addition, single crystals of **1** also can be obtained with 4,4′-bis(2-sulfonatostiryl)biphenyl) or 4,4′-bipyridine increased to 0.2 mmol in the initial reaction mixture.

Synthesis of [Co(4,4′-bipy)$_2$(L)]·2H_2O (2). A mixture of Co(CH_3COO)$_2$·4H_2O (0.0600 g, 0.241 mmol), 4,4′-bipyridine (0.0773 g, 0.495 mmol), Na_2L (0.1481 g, 0.2633 mmol), and water (10.0 mL, 556 mmol) was heated at 140 °C for 96 h. After the mixture was allowed to cool slowly to ambient temperature, orange prism-shaped crystals were obtained. The final pH of the solution was 4.66. The crystals were filtered, washed with distilled water, and dried at ambient temperature. The pattern of powder XRD was in accord with that simulated from single-crystal X-ray data, which indicated the homogeneous phase of the product. The yield was about 37% (0.0818 g) based on Co(CH_3COO)$_2$·4H_2O. Anal. Calcd for $C_{48}H_{40}N_4O_8S_2Co$ **2**: C 62.40, H 4.36, N 6.06. Found: C 61.64, H 4.52, N 6.01. IR (KBr pellet, cm^{-1}): 3535m (ν_{O-H}), 3057w(ν_{C-H}), 3026w($\nu_{C=C-H}$), 1605s, 1587m, 1537m, 1495m, 1464m, 1417m, 1225s, 1173s, 1132s, 1082s, 1022s, 970m, 831m, 810m, 798m, 750m, 721m, 636m, 611s, 577m, 538m.

Synthesis of [Co(4,4′-bipy)$_2$(H_2O)$_2$](4,4′-bipy)(L)·2H_2O (3). A mixture of Co(CH_3COO)$_2$·4H_2O (0.0249 g, 0.100 mmol), 4,4′-bipyridine (0.0773 g, 0.471 mmol), Na_2L (0.0581 g, 0.103 mmol), and water (10.0 mL, 556 mmol) was heated at 120 °C for 120 h. After the mixture was allowed to cool slowly to ambient temperature, orange prism-shaped crystals were obtained. The final pH of the solution was 5.55. The crystals were filtered, washed with distilled water, and dried at ambient temperature. The pattern of powder XRD was in accord with that simulated from single-crystal X-ray data, which indicated the homogeneous phase of the product. The yield was about 22% (0.0246 g) based on Co(CH_3COO)$_2$·4H_2O. Anal. Calcd for $C_{58}H_{52}N_6O_{10}S_2Co$ **3**: C 62.42, H 4.70, N 7.53. Found: C 61.77, H 4.93, N 7.16. IR (KBr pellet, cm^{-1}): 3400s(ν_{O-H}), 3067w(ν_{C-H}), 3050w(ν_{C-H}), 3020w($\nu_{C=C-H}$), 2395m, 1606s, 1566w, 1536m, 1496m, 1467m, 1414m, 1323w, 1242s, 1217s, 1170s, 1133m, 1071s, 1012s, 984w, 969w, 867w, 813s, 799m, 755m, 721m, 630m, 617s, 567m, 537m, 512m.

Synthesis of [Mn(4,4′-bipyH)$_2$(L)$_2$(H_2O)$_2$]·4H_2O (4). A mixture of Mn(CH_3COO)$_2$·4H_2O (0.0271 g, 0.110 mmol), 4,4′-bipyridine (0.0342 g, 0.220 mmol), Na_2L (0.0583 g, 0.103 mmol), and water (10.0 mL, 556 mmol) was heated at 120 °C for 96 h. After the mixture was allowed to cool slowly to ambient temperature, orange prism-shaped crystals were obtained. The final pH of the solution was 5.61. The crystals were filtered, washed with distilled water, and dried at ambient temperature. The pattern of powder XRD was

(3) (a) Dai, J. C.; Wu, X. T.; Fu, Z. Y.; Hu, S. M.; Du, W. X.; Cui, C. P.; Wu, L. M.; Zhang, H. H.; Sun, R. Q. *Chem. Commun.* **2002**, 12−13. (b) Tao, J.; Tong, M. L.; Shi, J. X.; Chen, X. M.; Ng, S. W. *Chem. Commun.* **2000**, 2043−2044. (c) Tong, M. L.; Chen, X. M.; Ye, B. H.; Ji, L. N. *Angew. Chem., Int. Ed.* **1999**, *38*, 2237−2240. (d) Song, J. L.; Zhao, H. H.; Mao, J. G.; Dunbar, K. R. *Chem. Mater.* **2004**, *16*, 1884−1889.7

(4) (a) Zhang, J.; Lin, W.; Chen, Z. F.; Xiong, R. G.; Abrahams, B. F.; Fun, H. K. *J. Chem. Soc., Dalton Trans.* **2001**, 1806−1808. (b) Wu, C. D.; Ngo, H. L.; Lin, W. *Chem. Commun.* **2004**, 1588−1589. (c) Han, L.; Hong, M. C.; Wang, R. H.; Luo, J. H.; Lin, Z. Z.; Yuan, D. Q. *Chem. Commun.* **2003**, 2580−2581. (d) Fun, H. K.; Raj, S. S. S.; Xiong, R. G.; Zuo, J. L.; Yu, Z.; You, X. Z. *J. Chem. Soc., Dalton Trans.* **1999**, 1915−1916. (e) Shi, J. M.; Xu, W.; Liu, Q. Y.; Liu, F. L.; Huang, Z. L.; Lei, H.; Yu, W. T.; Fang, Q. *Chem. Commun.* **2002**, 756−757.

(5) (a) Jüstel, T.; Nikol, H.; Ronda, C. *Angew. Chem., Int. Ed.* **1998**, *37*, 3084−3103. (b) Beurer, E.; Grimm, J.; Gerner, P.; Güdel, H. U. *J. Am. Chem. Soc.* **2006**, *128*, 3110−3111. (c) Czarnik, A. W. *Acc. Chem. Res.* **1994**, *27*, 302−308. (d) Royzen, M.; Durandin, A.; Young, V. G., Jr.; Geacintov, N. E.; Canary, J. W. *J. Am. Chem. Soc.* **2006**, *128*, 3854−3855. (e) Mansour, M. A.; Connick, W. B.; Lachicotte, R. J.; Gysling, H. J.; Eisenberg, R. *J. Am. Chem. Soc.* **1998**, *120*, 1329−1330. (f) Ma, Y. G.; Che, C. M.; Chao, H. Y.; Zhou, X. M.; Chan, W. H.; Shen, J. C. *Adv. Mater.* **1999**, *11*, 852−857.

(6) Stoll, J. M. A.; Giger, W. *Anal. Chem.* **1997**, *69*, 2594−2599.

Table 1. Crystallographic Data and Structural Refinements for **1**−**5**

	1	2	3	4	5
formula	$C_{38}H_{32}N_2O_8S_2Cd$	$C_{48}H_{40}N_4O_8S_2Co$	$C_{58}H_{52}N_6O_{10}S_2Co$	$C_{76}H_{70}N_4O_{18}S_4Mn$	$C_{46}H_{42}N_{12}O_6S_2Zn_2$
color	orange	orange	orange	orange	orange
fw	821.18	923.89	1116.11	1510.54	1053.78
space group	$P2_1/n$	$P\bar{1}$	$P2_1/n$	$Pbcn$	$Pbcn$
cryst size (mm^3)	0.50 × 0.25 × 0.25	0.20 × 0.20 × 0.20	0.30 × 0.20 × 0.10	0.35 × 0.22 × 0.20	0.55 × 0.30 × 0.10
a (Å)	11.253(3)	10.144	11.8313(7)	31.9128(16)	26.1518(11)
b (Å)	19.832(4)	10.6094(3)	15.7956(8)	10.5868(4)	17.4539(9)
c (Å)	15.927(3)	11.3345(5)	15.0349(9)	20.0074(9)	10.3435(5)
α (deg)	90	84.816(15)	90	90	90
β (deg)	102.812(2)	75.745(12)	104.773(3)	90	90
γ (deg)	90	67.251(9)	90	90	90
V ($Å^3$)	3465.9(13)	1090.28(6)	2716.9(3)	6759.6(5)	4721.3(4)
Z	4	1	2	4	4
ρ_{calcd} (g cm^3)	1.574	1.407	1.364	1.484	1.483
μ (mm^{-1})	0.808	0.549	0.458	0.398	1.167
observed reflns	7344	3999	5356	7320	4944
params	476	358	453	487	307
GOF on F^2	1.160	1.071	1.108	1.185	1.115
$R1$, $wR2$ ($I > 2\sigma(I)$)[a]	0.0401/ 0.0835	0.0481/0.1122	0.0479/0.1101	0.0532/0.1197	0.0434/0.1087
$R1$, $wR2$ (all data)	0.0450/0.0864	0.0625/0.1221	0.0580/ 0.1154	0.0569/0.1216	0.0479/0.1119
ρ_{max}, ρ_{min} e × $Å^{-3}$	1.067, −0.445	0.376, −0.454	0.365, −0.423	0.477, −0.482	0.437,-0.376

[a] $R1 = \sum(||F_o| - |F_c||)/\sum |F_o|$, $wR2 = \{\sum w [(F^2_o - F^2_c)]/\Sigma w [(F^2_o)^2]\}^{0.5}$.

accord with that of simulated from single-crystal X-ray data, which indicated the homogeneous phase of the product. The yield was about 29% (0.0224 g) based on Na_2L. Anal. Calcd for $C_{76}H_{70}N_4O_{18}S_4Mn$ **4**: C 60.43, H 4.67, N 3.71. Found: C 60.33, H 4.80, N 3.55. IR (KBr pellet, cm^{-1}): 3431s(ν_{O-H}), 3230w(ν_{N-H}), 3068w(ν_{C-H}), 3028w($\nu_{C=C-H}$), 1635w, 1605m, 1558w, 1522w, 1493m, 1464m, 1416m, 1338w, 1286w, 1201vs, 1167vs, 1157s, 1136s, 1084s, 1043m, 1016s, 982w, 962m, 951w, 858w, 810s, 764m, 748m, 727m, 700m, 615s, 575m, 538m.

Synthesis of $[Zn_2(Im)_2(ImH)_4](L)$ (5) (ImH = imidazole). A mixture of $Zn(CH_3COO)_2 \cdot 2H_2O$ (0.1010 g, 0.4602 mmol), Na_2L (0.1396 g, 0.2482 mmol), imidazole (ImH) (0.2001 g, 2.939 mmol), and H_2O (10.0 mL, 556 mmol) was heated at 120 °C for 144 h. After the mixture was cooled slowly to ambient temperature, orange prism-shaped crystals were obtained. The final pH of the solution was 7.80. The crystals were filtered, washed with distilled water, and dried at ambient temperature. A suitable crystal was selected for single-crystal X-ray diffraction studies. The pattern of experimental powder XRD was in accord with those of simulated from single-crystal X-ray data, which indicated the homogeneous phase of the product. The yield was about 56% (0.1354 g) based on $Zn(CH_3COO)_2 \cdot 2H_2O$. Anal. Calcd for $C_{46}H_{42}N_{12}O_6S_2Zn_2$ **7**: C 52.56, H 4.03, N 16.0. Found: C 52.26, H 3.93, N 15.87. IR (KBr pellet, cm^{-1}): 3136m(ν_{N-H}), 3117s(ν_{N-H}), 3061(ν_{C-H}), 3030w($\nu_{C=C-H}$), 2865m, 1627w, 1590w, 1543m, 1497m, 1467m, 1331m, 1271m, 1230s, 1221s, 1202s, 1166vs, 1132s, 1091s, 1081s, 1072s, 1014s, 966m, 953m, 922w, 881w, 827m, 805m, 776m, 756m, 752m, 698m, 672m, 659s, 617s, 597m, 572m, 562m, 536m.

Single-crystal X-ray Diffraction. X-ray data were collected on a Rigaku Mercury CCD/AFC diffractometer using graphite-monochromated Mo Kα radiation (λ(Mo Kα) = 0.71073 Å) at 293(2) K (for **1**, **3**, **4**, **5**) and 130(2) K (for **2**). Data were reduced with *CrystalClear* version 1.3. These structures were solved by direct methods and refined by full-matrix least-squares techniques on F^2 using *SHELXTL-97*.[7] All non-hydrogen atoms were treated anisotropically. In **1**, hydrogen atoms that bonded to carbon atoms were generated geometrically. Whereas hydrogen atoms of coordinated water molecules in **1** were from the difference Fourier map and fixed with O−H = 0.96 and H···H = 1.52 Å. In **2**, hydrogen atoms that bonded to carbon were from the difference Fourier map and were with the fixed isotropic thermal parameter, and no attempt was made to locate those of the free water molecule. All of the hydrogen atoms in **3** were from the difference Fourier map and were with the fixed isotropic thermal parameter. In **4**, hydrogen atoms that bonded to carbon atoms were generated geometrically. Whereas the hydrogen atom that bonded to nitrogen atoms of 4,4′-bipy group, as well as hydrogen atoms of the coordinated water molecules, it was from the difference Fourier map with the fixed isotropic thermal parameter. No attempt was made to locate hydrogen atoms of free water molecules. All of the hydrogen atoms in **5** were generated geometrically. Crystallographic data and structural refinements for **1**−**5** are summarized in Table 1. CCDC-297562 (for **1**), 634825−634827 (for **2**-**4**, respectively), and 834830 (for **5**).

Results and Discussion

Structure Descriptions. Single-crystal X-ray diffraction of **1** reveals that binuclear $[Cd_2]$ secondary building units (SBUs) are bridged by 4,4′-bipys into a 2D cationic framework, which is further penetrated by **L** anions into an organic−inorganic hybrid layer (Figure 1). The Cd(II) atom locates in a $[CdN_2O_4]$ distorted-octahedral coordination geometry, which is defined by two nitrogen atoms from two 4,4′-bipys (N1 and N2), two oxygen donors from two **L** anions (O1 and O3a), and two aqua molecules (O7 and O8). The neighboring two $[CdN_2O_4]$ octahedrons contact each other through two {−O−S−O−} bridges into a binuclear $[Cd_2]$ SBU, which is similar to those in the dinuclear cluster [Cd(1,4,8,11-tetraazacyclotetradecane) (1,5-naphthahlenedisulfonate)] and the 1D coordination polymer $\{[Cd_2(isoincotinamide)_4(H_2O)_3(4,4'\text{-phenyletherdisulfonate})_2] \cdot 2H_2O\}$.[8] The cross-linkage of $[Cd_2]$ SBUs by 4,4′-bipys leads to a 2D framework built from bricklike motifs with sizes of about 1.6 × 1.1 nm^2 (calculated from the distance between Cd(II)

(7) Sheldrick, G. M. *SHELXT 97, Program for Crystal Structure Refinement*; University of Göttingen: Göttingen, Germany, 1997.

(8) Chen, C. H.; Cai, J. W.; Liao, C. Z.; Feng, X. L.; Chen, X. M.; Ng, S. W. *Inorg. Chem.* **2002**, *41*, 4967−4974.

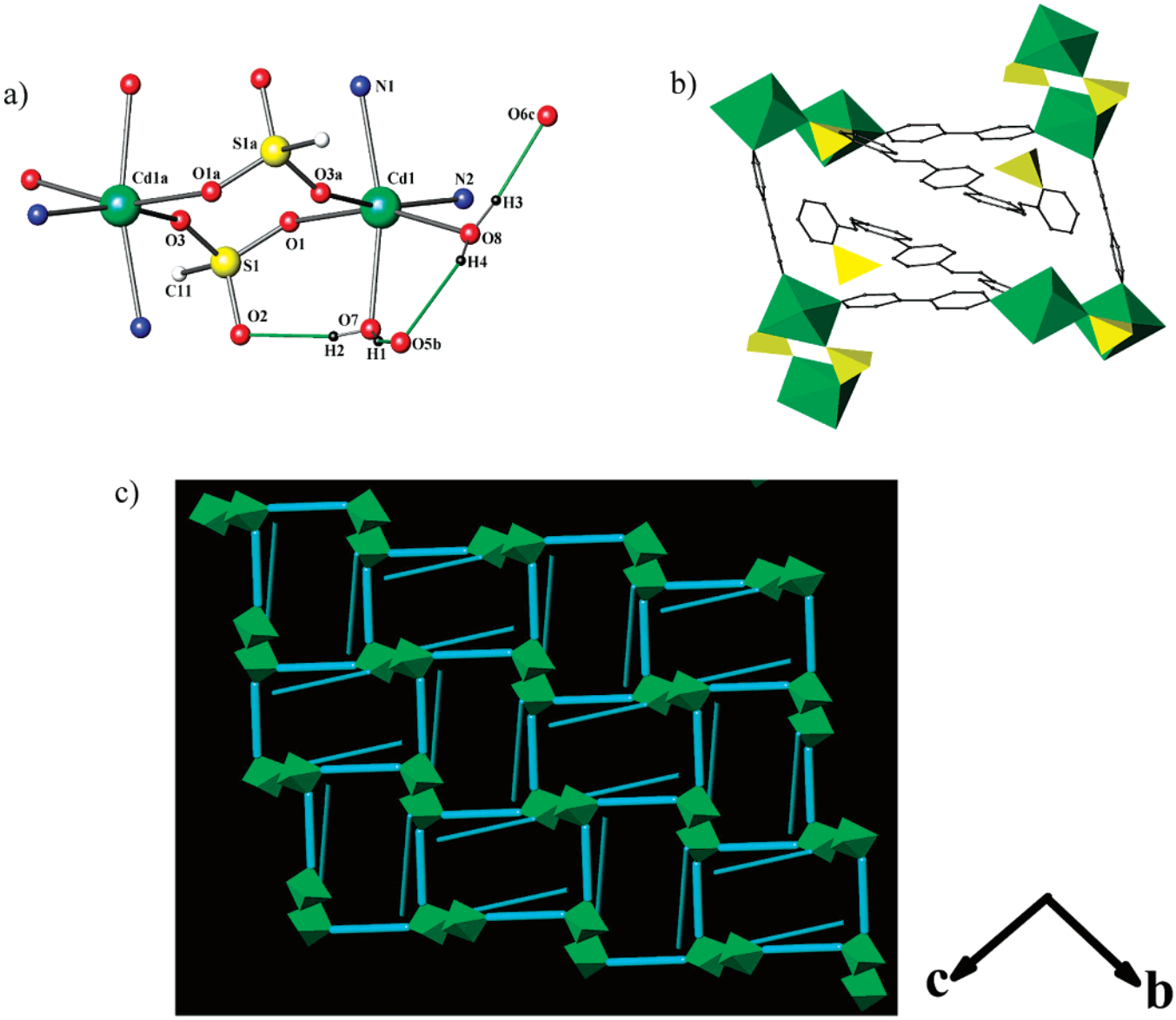

Figure 1. (a) Ball-stick representation of the binuclear [Cd_2] unit in **1**. The green thin line indicates hydrogen bonds. Selected bond lengths (Å) and angles (°): Cd1−O1 2.3497(18), Cd1−O3a 2.3805(19), Cd1−O7 2.279(2), Cd1−O8 2.320(2), Cd1−N1 2.291(2), Cd1−N2 2.297(2); O1−Cd1−O3a 102.94(7), O1−Cd1−O7 84.61(7), O1−Cd1−O8 161.39(8), O1−Cd1−N1 87.90(7), O1−Cd1−N2 92.63(7), O3a−Cd1−O7 88.04(8), O3a−Cd1−O8 79.94(7), O3a−Cd1−N1 80.31(8), O3a−Cd1−N2 161.94(8), O7−Cd1−O8 77.07(8), O7−Cd1−N1 164.40(9), O7−Cd1−N2 102.66(9), O8−Cd1−N1 110.67(8), O8−Cd1−N2 88.24(8), N1−Cd1−N2 91.32(8). Symmetry codes: a: $2 - x, 2 - y, 1 - z$; b: $^1/_2 - x, ^1/_2 + y, ^1/_2 - z$; c: $^1/_2 + x, ^3/_2 - y, ^1/_2 + z$. (b) Polyhedral view of the bricklike motif in **1**. Green octahedron, [CdN_2O_4]; yellow tetrahedron, [SCO_3]. (c) View of 2D hybrid layer in **1**. Green octahedron, [CdN_2O_4]; thin line, **L**; thick line, 4,4′-bipy.

atoms), which is larger than the square motif in [Zn(4,4′-bipy)$(H_2O)_4$][Zn(4,4′-bipy)$_{1.5}$(L)$(H_2O)_2$]·(L)·6H_2O.[2f] As a result, two **L** anions can slantways penetrate the bricklike motif. However, only one **L** anion is allowed to penetrate the square motif in the above-mentioned zinc polymer.[2f] Besides electrostatic interaction, each **L** anion interacts to the 2D framework with two covalent bonds (Cd1−O1 and Cd1−O3) and one hydrogen bond (O2···O7 = 2.713(3) Å) via the coordinated SO_3 terminal group. It is interesting that the **L** anion also contacts the framework through offset face-to-face $\pi-\pi$ stacking interactions between 4,4′-bipy and the biphenyl of the **L** anion with a ∼3.40 Å distance of separation and a 3.67 Å centroid−centroid distance (Figure S1 in the Supporting Information).[9] The uncoordinated SO_3 terminal group plays an important role in packing neighboring layers into a 3D structure through three hydrogen bonds: O5···O7 = 2.771(3), O5···O8 = 2.837(3), and O6···O8 = 2.657(3) Å.

In **2**, the Co(II) atom is coordinated to four nitrogen atoms from four equivalent 4,4′-bipys (N1, N1a, N2, and N2a) and two oxygen donors (O4 and O4a) from two equivalent **L** anions, resulting in a slightly distorted [CoN_4O_2] octahedron geometry (Figure 2). Each Co(II) atom is linked by four 4,4′-bipys to form a 4^4 cationic framework consisting of a squarelike unit with sizes about 1.1 × 1.1 nm^2 (calculated from the distance of neighboring cobalt atoms), which is similar to that in the above-mentioned zinc polymer.[2f] **L** anion attaches to the framework with two covalent bonds

(9) Janiak, C. *J. Chem. Soc., Dalton Trans.* **2000**, 3885−3896.

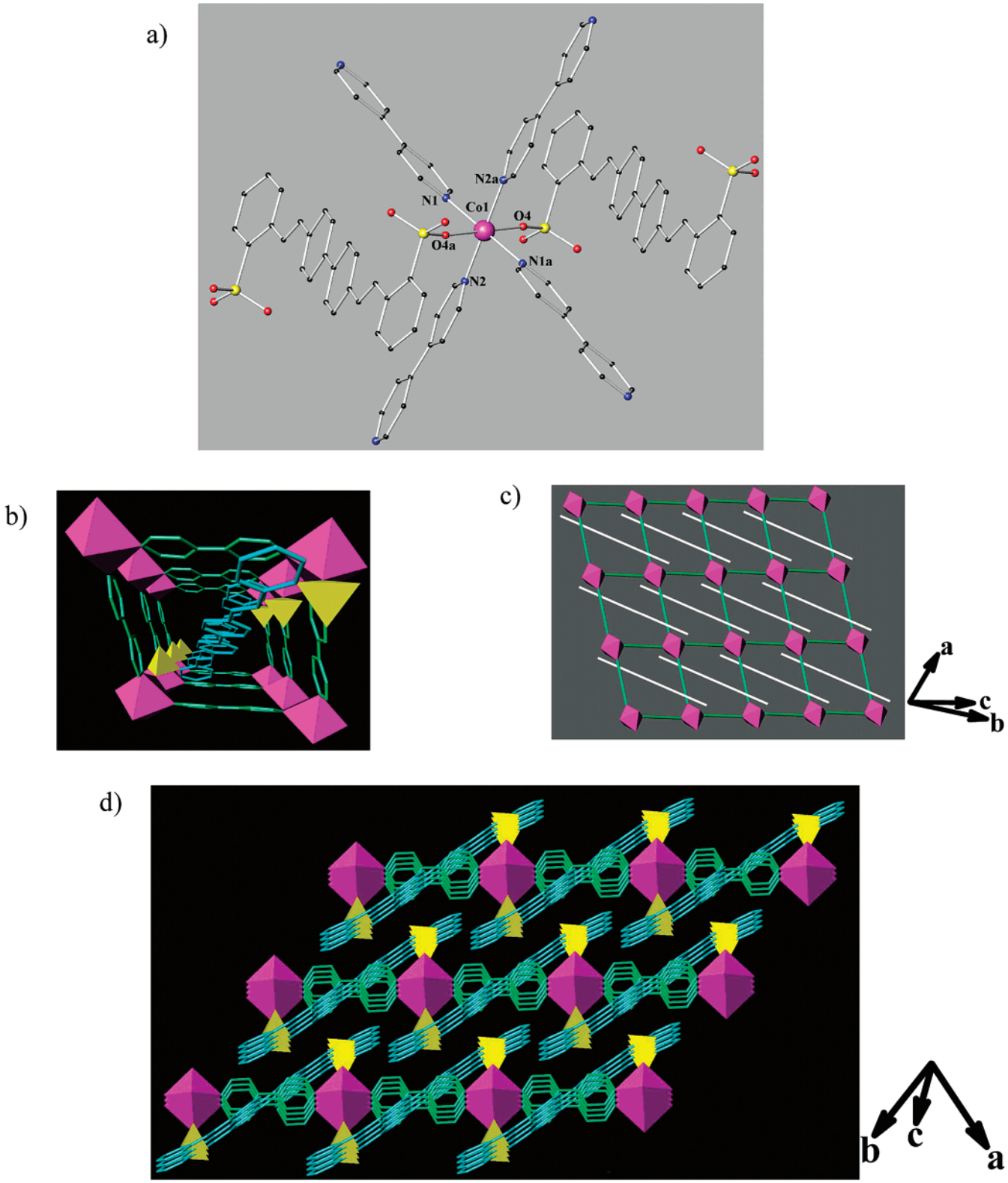

Figure 2. (a) Ball-stick representations show the coordination environment of Co(II) atom in **2**. Selected bond lengths (Å) and angles (°): Co1−O4 2.095(2), Co1−N1 2.208(2), Co1−N2 2.137(2); O4−Co1−N1 90.37(7), O4−Co1−N2 92.27(7), N1−Co1−N2 94.46(7). Symmetry code: a: $-x, -y, -z$. (b) Perspective view shows the 1D channel directed by **L** anions down *b* axis in **2**. (c) Pack views show hybrid layer, and (d) the 3D structure in **2**. Rose octahedron, $[CoN_4O_2]$; yellow tetrahedron, $[SCO_3]$; green line, 4,4′-bipy; white line, **L**.

(Co1−O4) through both terminal SO_3 groups. As a result, each **L** anion interpenetrates slanting into each squarelike unit to form an organic−inorganic hybrid layer. On one hand, between neighboring layers **L** anions are interlaced into a gearlike mode to strengthen the van der Waals interaction, which is the main force to pack the hybrid layers into a 3D structure. On the other hand, the squarelike units are directed by **L** anions into a 1D channel along the *b* axis.

As shown in Figure 3, the Co(II) atom in **3** is in a $[CoN_4O_2]$ octahedron geometry, which is defined by four

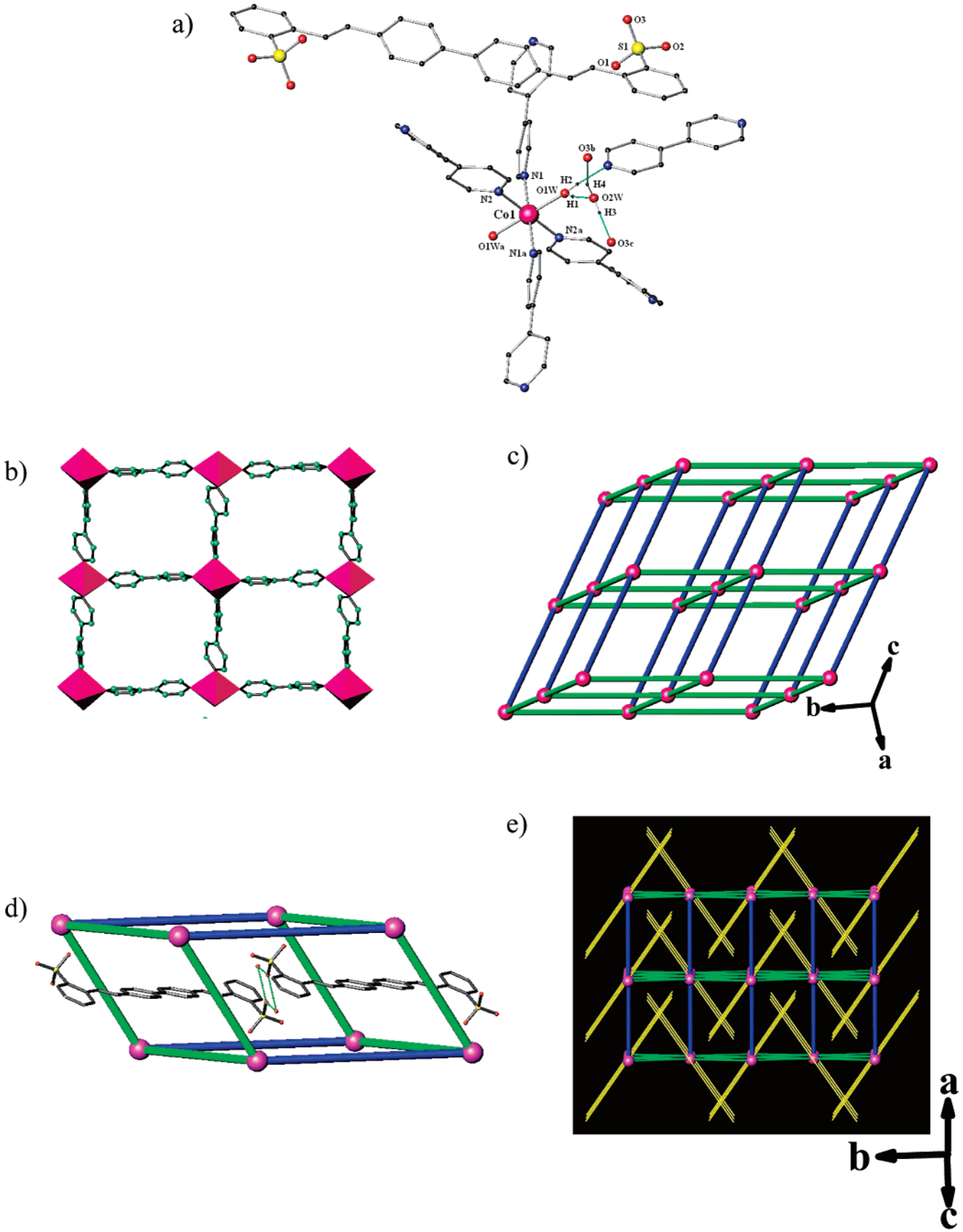

Figure 3. (a) Ball-stick representations show the coordination environment of cobalt and sulfur in **3**. Selected bond lengths (Å) and angles (°): Co1−O1W 2.0379(15), Co1−N1 2.2001(15), Co1−N2 2.2103(15); O1W−Co1−N1 88.18(7), O1W−Co1−N2 89.40(6), N1−Co1−N2 88.44(6). Symmetry codes: a: $-x, -y, -z$; b: $^1/_2 + x, ^1/_2 - y, ^1/_2 + z$; c: $^1/_2 - x, -^1/_2 + y, -^1/_2 - z$. (b) Polyhedral views show the 4^4 framework in **3**. Rose octahedron, [CoN_4O_2]. (c) 3D pcu-like framework, (d) the parallelepiped-like unit, and (e) the 3D framework encapsulating **L** anions in **3**. Green line, 4,4′-bipy; blue line, water-4,4′-bipy-water; yellow line, **L** anion; rose ball, cobalt.

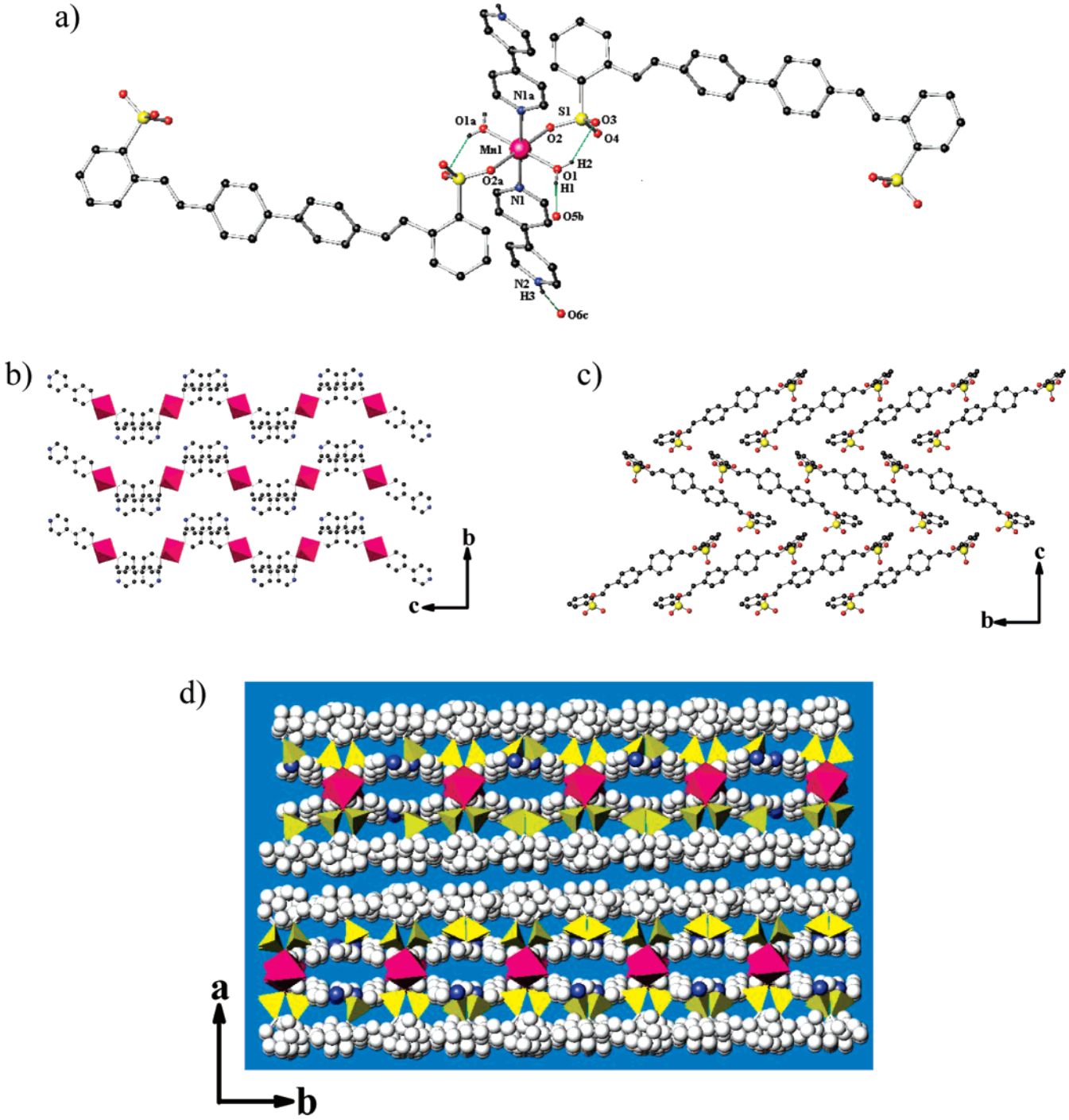

Figure 4. (a) Ball-stick representations show the coordination environment of manganese and sulfur in **4**. Selected bond lengths (Å) and angles (°): Mn1−O1 2.170(2), Mn1−O2 2.1572(16), Mn1−N1 2.3023(19); O1−Mn1−O2 90.97(7), O1−Mn1−N1 90.40(7), O2−Mn1−N1 86.22(7). Symmetry codes: a: $-x, 2-y, 1-z$; b: $-x, 1+y, {}^{1}/_{2}-z$; c: $-x, 1-y, -z$. Polyhedral and ball-stick views show (b) the cationic layer, (c) the anionic layer, and (d) the sandwichlike structure in **4**. Rose octahedron, [MnN_2O_4]; yellow tetrahedron, [SCO_3].

nitrogen atoms (N1, N1a, N2, and N2a) from four equivalent 4,4′-bipys and two aqua ligands (O1W and O1Wa). Like that in **2**, the cross-linkage of Co(II) atoms by 4,4′-bipys leads to a 4^4 cationic framework constructed from squarelike motifs. The 4^4 framework is further bridged by the free 4,4′-bipy through hydrogen bonds with the coordinated aqua molecules (O1W···N3 = 2.674(3) Å), to form a pcu-like 3D cationic framework. The 3D framework is built up from parallelepiped-like unit with sizes of about 1.1 × 1.1 × 1.5 nm^3 (calculated from the distance to neighboring cobalt atoms). As expected, the **L** anion does not take part in coordination because of excessive 4,4′-bipy in the reaction mixture. Neighboring **L** anions are linked by two free water molecules into an anionic chain via hydrogen bonds (O2W···O3b = 2.724(3), O2W···O3c = 2.710(3) Å). The anionic chain is encapsulated into the squarelike channel of the 3D framework via electrostatic interaction, as well as by hydrogen bonds between the coordinated aqua ligands and the free water molecules (O1W···O2W = 2.606-(3) Å).

The asymmetric unit of **4** consists of one Mn(II) atom, one **L** anion, one monoprotonated 4,4′-bipy (denoted as 4,4′-bipyH), one coordinated aqua ligand, and two free water molecules (Figure 4). Mn(II) combines with two 4,4′-bipyHs (N1 and N1a), two **L** anions (O2 and O2a), and two coordinated aqua ligands (O1 and O1a) into a $[Mn(4,4'\text{-bipyH})_2(L)_2(H_2O)_2]$ fragment. On one hand, the $[Mn(4,4'\text{-bipyH})_2(H_2O)_2]^{4+}$ cationic fragment is sandwiched by **L** anions into sandwichlike hybrid layer through one covalent bond (Mn1−O2) and three hydrogen bonds: O1···O3 = 2.944(3), O1···O5 = 2.846(3), and N2···O6 = 2.766(3) Å. Neighboring $[Mn(4,4'\text{-bipyH})_2(H_2O)_2]^{4+}$ cationic fragments interact with each other through slide face-to-face $\pi-\pi$ stacking interactions between bipyridines with a separated distance of about 3.5 Å and a centrosoid-to-centrosoid distance of about 4.2 Å, resulting in an infinite zigzag cationic chain.[9] On the other hand, on the *bc* plane, the aggregation of **L** anions is a like scalelike layer.

In **5**, the Zn(II) atom is in a $[ZnN_4]$ slightly distorted tetrahedral coordination geometry, which is surrounded by two imidazoles (N3 and N5) and two deprotonated imidazoles (N1 and N2) (Figure 5). The tetrahedrons are bridged by the deprotonated imidazoles into a twisted $[Zn(Im)(ImH)_2]^+$ cationic chain. The $[Zn(Im)(ImH)_2]^+$ chains are further combined by **L** anions through hydrogen bonds (O1···N4 = 2.840(3), O2···N6 = 2.803(3) Å), and by van der Waals interactions into a honeycomb-like structure, possessing 1D channels with a cross-distance of about 1.6 nm. Each channel encapsulates two parallel **L** anionic chains.

Magnetic Property. The temperature dependence of the $\chi_m T$ product, magnetic susceptibility (χ_m), and inverse magnetic susceptibility ($1/\chi_m$) for **2** at 5 KOe from 2 to 308 K are shown in Figure 6. Upon cooling, the $\chi_m T$ product decreases gradually from 3.05 emu K mol^{-1} at 308 K to 1.71 emu K mol^{-1} at 2 K. By using the equation $\mu_{eff} = (8\chi_m T)^{1/2}$, at 308 K the effective magnetic moment per cobalt atom ($\mu_{eff} = 4.95\ \mu_B$) is obviously higher than the reported spin-only value of 3.87 μ_B. However, the value lies in the range of 4.4−5.2 μ_B due to the orbital contribution at room temperature.[10] Between 20 and 308 K, the magnetic susceptibility consists well with the Curie−Weiss law [$\chi_m^{-1} = 5.0(1) + 0.3098(6)$ T] ($r = 0.9999$), with $C = 3.23$ emu K mol^{-1} and $\theta = -16.1$ K. The negative θ value together with the continuous decrease in $\chi_m T$ upon cooling indicate the presence of antiferromagnetic interactions.

Thermal Stabilities. Thermal behaviors of **1**, **2**, **4**, and **5** were investigated using thermogravimetric analysis (TGA) and powder XRD. As shown in Figure 7, the TGA curve of **1** exhibits two mild weight-loss steps from 87 °C up to 204 °C, with the observed weight loss of 4.37% corresponding to the release of two coordinated aqua molecules per formula (Calcd 4.39%). Then, little weight loss appears up to 400 °C. Furthermore, polycrystalline **1** was previously annealed at 200, 250, and 280 °C under an air atmosphere for 2 h. Except for a new peak appearing with a 2θ of about 6.85 ° for releasing the coordinated aqua molecules, PXRD patterns are all agreement with those of the pristine solid,

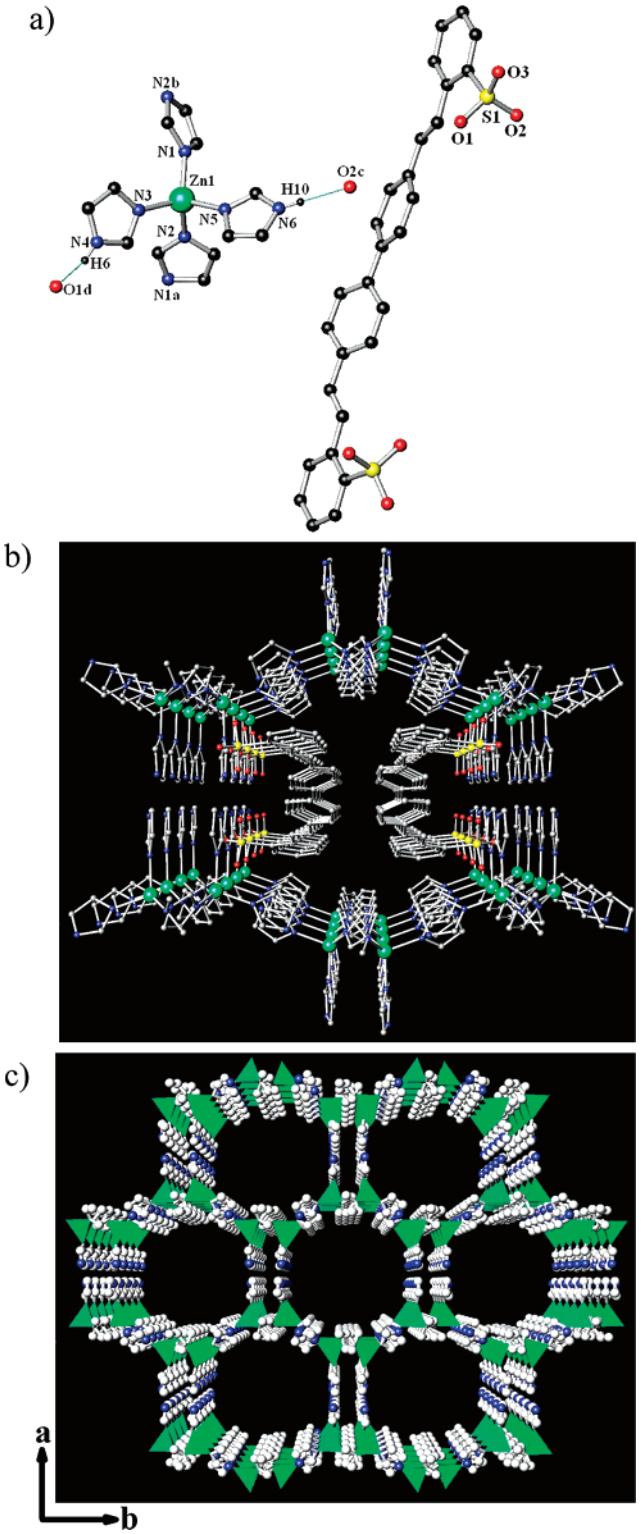

Figure 5. (a) Ball-stick representations show the coordination environment of zinc and sulfur in **5**. Selected bond lengths (Å) and angles (°): Zn1−N1 1.973(2), Zn1−N2 1.995(2), Zn1−N3 1.9904(19), Zn1−N5 2.036(2); N1−Zn1−N2 111.71(9), N1−Zn1−N3 115.53(8), N1−Zn1−N5 109.74(8), N2−Zn1−N3 106.66(8), N2−Zn1−N5 104.65(9), N3−Zn1−N5 107.93(9). Symmetry codes: a: $x, 1-y, -1/2+z$; b: $x, 1-y, 1/2+z$; c: $-x, y, 1/2-z$; d: $1/2-x, 3/2-y, -1/2+z$. (b) Ball-stick view shows the 1D channel encapsulating **L** anions. (c) Perspective view shows the 3D honeycomb-like porous structure.

(10) (a) Sanz, F.; Parada, C.; Rojo, J. M.; Ruiz-Valero, C. *Chem. Mater.* **2001**, *13*, 1334−1340. (b) Carlin, R. l. *Magneto-chemistry*; Springer-Verlag: New York, 1986.

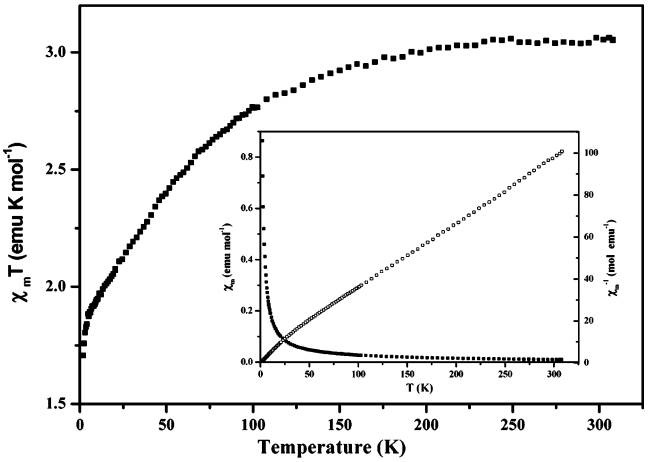

Figure 6. Thermal dependence of the $\chi_m T$ (solid squares) product for **2**. The inset shows magnetic susceptibility (χ_m, solid squares) and inverse magnetic susceptibility ($1/\chi_m$, open squares) plotted as a function of temperature for **2**.

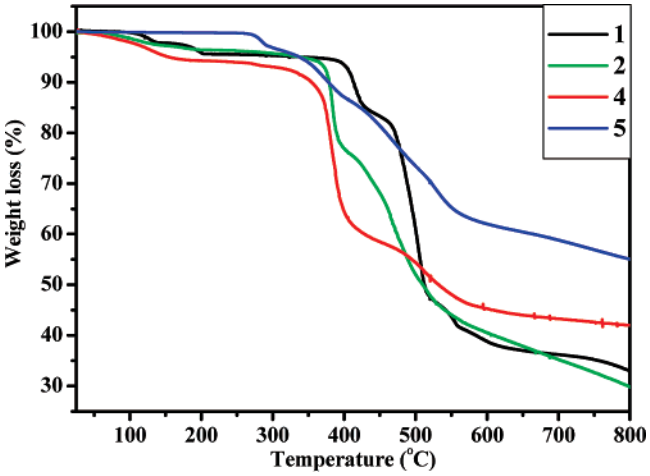

Figure 7. TGA curves for **1**, **2**, **4**, and **5**.

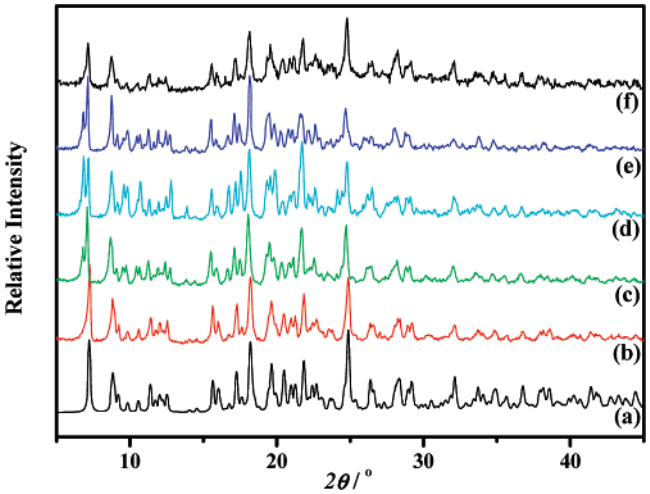

Figure 8. PXRD patterns of **1** simulated from single-crystal X-ray data (a), experimental data (b), and polycrystalline of **1** was annealed at 200 °C (c), 250 °C (d), and 280 °C (e) for 2 h under an air atmosphere. PXRD pattern of polycrystalline **1** was previously annealed at 200 °C for 2 h under an air atmosphere and then immersed in distilled water for about 2 days (f).

indicating the retention of the framework (Figure 8). It is interesting that the new peak will disappear if the dehydrated

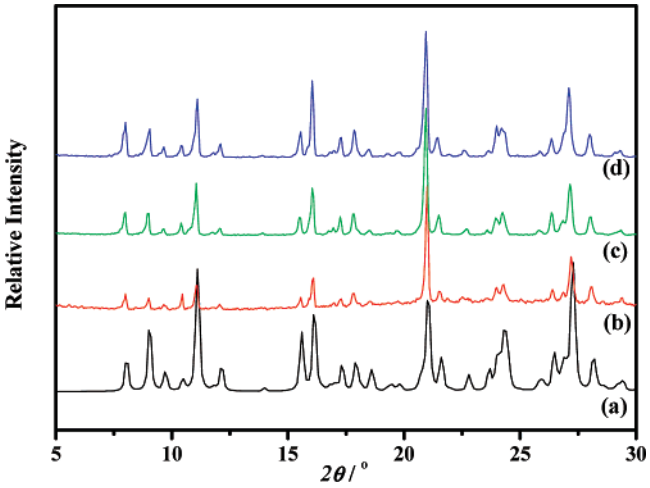

Figure 9. PXRD patterns of **2** simulated from X-ray single-crystal data (a), experimental data (b), and polycrystalline **2** was previously annealed at 200 °C (c) and 250 °C for 2 h under an air atmosphere.

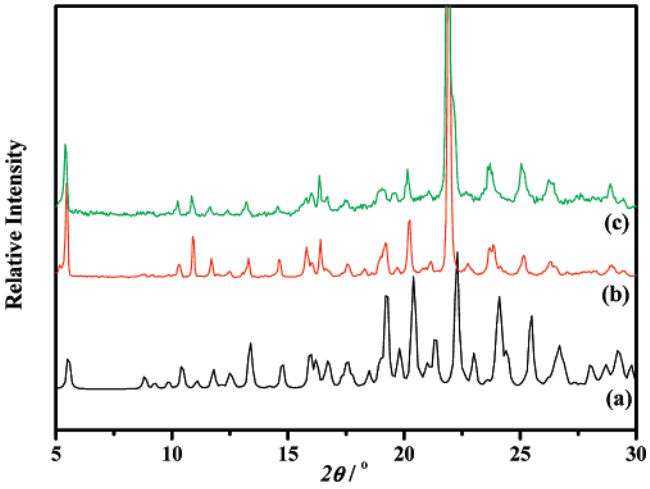

Figure 10. PXRD patterns of **4** simulated from X-ray single-crystal data (a), experimental data (b), and polycrystalline **4** was preciously annealed at 200 °C for 2 h under an air atmosphere (c).

powder is immersed in distilled water for about 2 days, which suggests that the coordinated waters can be reversibly removed and recovered. The TGA diagram of **2** displays a small weight-loss step in the range of 50−200 °C, with the observed weight loss of 3.5% matching the calculated value (3.9%), attributed to the loss of two free water molecules per formula. Following that, there is little weight loss up to 360 °C. The TGA curve of **4** reveals that an initial weight-loss step starts from room temperature and completes at 200 °C. The observed weight loss of 5.7% is smaller than the theoretical value (7.1%) for the loss of four free water molecules and the two coordinated water molecules per formula. The deviation may be due to the easy loss of free water under ambient temperature. Little weight appears up to 300 °C. The TGA diagram of **5** illustrates there is little weight loss below 260 °C. In addition, PXRD patterns suggest that the frameworks of **2**, **4**, and **5** are stable after they anneal at 300, 200, and 250 °C for 2 h under an air atmosphere, respectively (Figure 9-11).

Luminescent Properties. Solid-state luminescent properties of solids **1**−**2**, **4**, and **5** were investigated under ambient

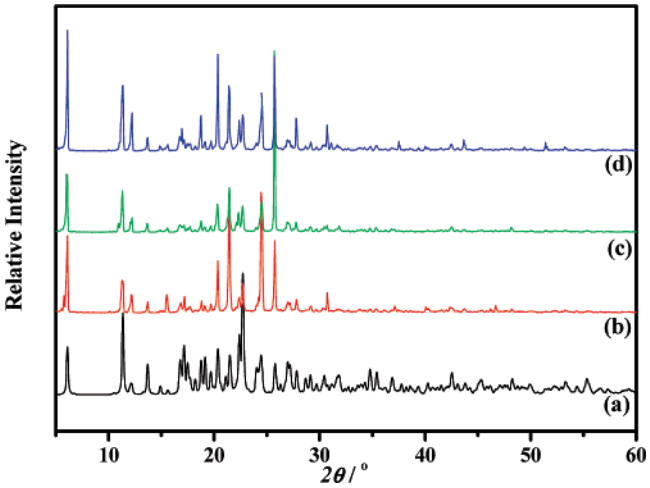

Figure 11. PXRD patterns of **5** simulated from X-ray single-crystal data (a), experimental data (b), and polycrystalline **5** was preciously annealed at 200 °C (c) and 250 °C for 2 h under an air atmosphere.

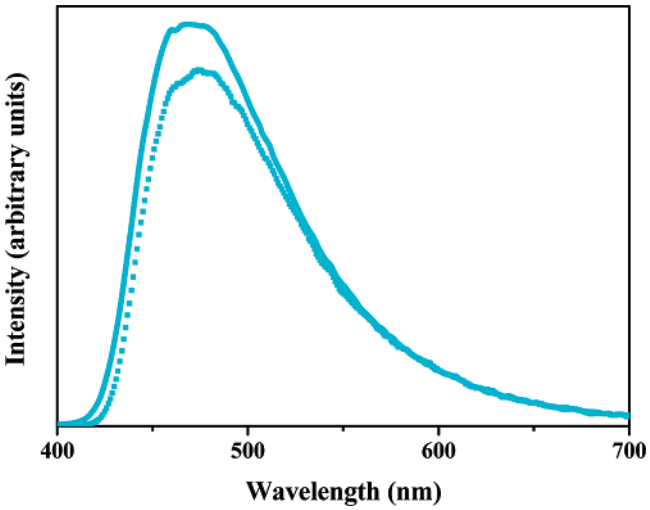

Figure 12. Normalized solid-state fluorescence emission spectra of **1** (solid line) and the dehydrated **1** (dot line), which was previously annealed at 200 °C under an air atmosphere for 2 h.

temperature. The diffuse reflectance spectrum of **2** shows a very broad absorption band between 250 and 600 nm, which may quench the luminescence through self-absorption. As a result, no luminescent emission for **2** can be detected under our experiment conditions. **3** also displays no emission under a UV lamp with an excitation of 254 or 365 nm. In contrast, **1**, **4**, and **5** possess intriguing fluorescent emissions. **1** could emit a bright blue-green luminescence with a peak maximum band at 470 nm ($\lambda_{ex} = 370$ nm), which is obviously different from the blue luminescence for the reported coordination polymers (Figure 12).[2c−e,3,4a,b] The full width at half-maximum (fwhm) is 92 nm. Under the excitation of 278 nm, **1** displays a slightly brighter blue-green emission than those of **1** excited at 370 or 410 nm. This is in agreeance with the broad excitation spectrum with a maximum peak at 278 nm (Figure S2 and S3 in the Supporting Information). The emission probably originates from the interligand $\pi-\pi^*$ transition between **L** and 4,4′-bipy, as well as from the ligand-centered $\pi-\pi^*$ transition of **L** and 4,4′-bipy.[2c,d,4] Similar to those reported in previous work, the peak band

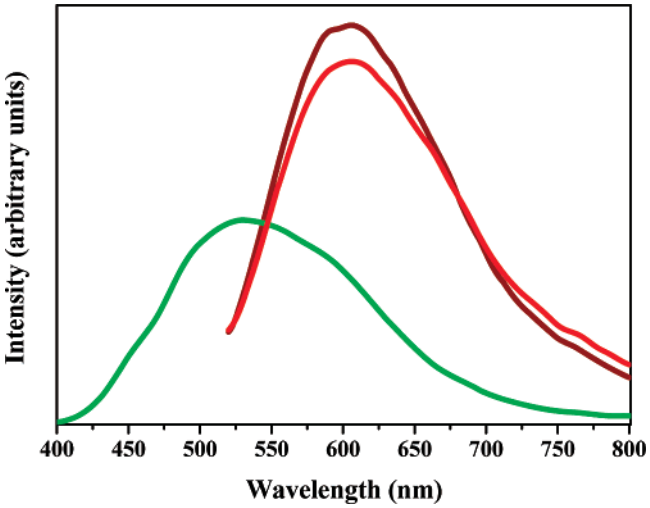

Figure 13. Normalized solid-state fluorescence emission spectra of **4** excited at 280 nm (green line) and 500 nm (dark red), as well as dehydrated **4** excited at 500 nm (red line), which was preciously annealed at 200 °C under an air atmosphere for 2 h.

of **1** exhibits 18 and 10 nm bathochromic shifts compared to those of $\mathbf{Na_2L}$ ($\lambda_{max} = 452$ nm, excited at 410 nm) and 4,4′-bipy ($\lambda_{max} = 460$ nm, excited at 345 nm) (Figure S4 of the Supporting Information).[2b−d,2f,3d] Preliminary experimental results reveal that its fluorescence intensity is about 19% that of $\mathbf{Na_2L}$. The lifetime for $\lambda_{ex,em} = 397\ 480$ nm is 13.6(4) ns, which is only about one-third of that of the above-mentioned zinc polymer (39 ns for $\lambda_{ex,em} = 426\ 542$ nm).[2f] Dehydrated **1**, which was previously annealed at 200 °C under an air atmosphere for 2 h, shows a similar emission to that of pristine **1**. This result is in agreement with the retention of the framework for the dehydrated phase. However, the fluorescence intensity (16% that of $\mathbf{Na_2L}$) and lifetime (11.3(2) ns for $\lambda_{ex,em} = 370\ 480$ nm) of dehydrated **1** are slight weaker and shorter than those of pristine **1**. In addition, if polycrystalline **1** was annealed at 250 and 280 °C under an air atmosphere for 2 h, a bright blue-green emission can also be seen with the naked eye under a UV lamp, with an excitation of 254 or 365 nm. The above results imply that **1** is an attractive candidate for potential application because luminescent materials transfer ultraviolet radiation to blue-green light.

As shown in Figure 13, **4** features tunable luminescence between dark red and weak green. On one hand, **4** has a dark-red luminescence with an emission maximum at 606 nm, a fwhm of 146 nm, and a lifetime of 1.78(7) ns (monitored at 590 nm) under an excitation of 500 nm, which is also obvious different from blue luminescence for the reported coordination polymers (Figure 12).[2c−e,3,4a,b] The emission may be attributed to ligand-to-metal charge transfer due to a Mn^{2+} ion, which is an important luminescent activator in many red phosphors.[2a,2d,3b,11] It is attractive that the peak band exhibits 154 and 146 nm bathochromic shifts compared to those of $\mathbf{Na_2L}$ and 4,4′-bipy, respectively. On the other hand, **4** also shows a weak green emission under

(11) (a) García-Hipólito, M.; Alvarez-Fregoso, O.; Martínez, E.; Falcony, C.; Aguilar-Frutis, M. A. *Optic. Mater.* **2002**, *20*, 113−118. (b) Wang, J.; Wang, S. B.; Su, Q. *J. Mater. Chem.* **2004**, *14*, 2569−2574.

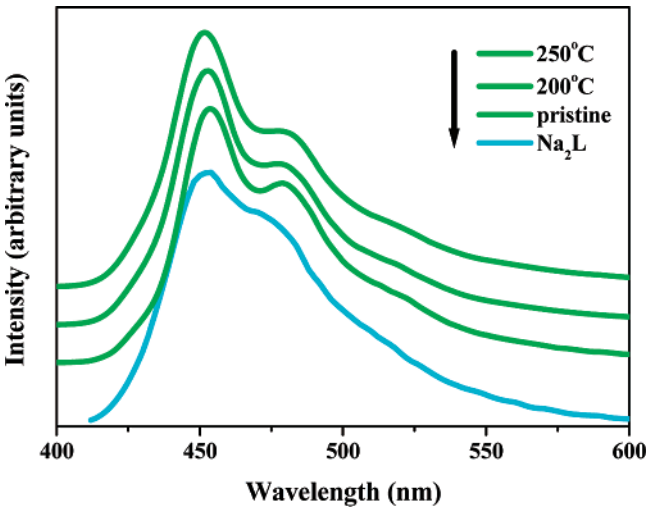

Figure 14. Normalized solid-state fluorescence emission spectra of **5**, Na_2L, and polycrystalline **7** was previously annealed at 200 and 250 °C under an air atmosphere for 2 h.

an excitation wavelength at 280 nm. The profile is very broad (fwhm of 166 nm) with a peak band at 530 nm. The weak-green emission of **4** probably originates from the ligand-centered $\pi-\pi^*$ transition of **L**.[2c,d,4] Dehydrated **4**, which was previously annealed at 200 °C under an air atmosphere for 2 h, displays dark-red luminescence similar to that of pristine **4**. This result also is in accordance with the retention of the framework for the dehydrated phase. The lifetime of dehydrated **4** is 2.57(8) ns ($\lambda_{ex,em}$ = 500, 600 nm), which is 0.79 ns longer than that of pristine **4**. Corresponding excitation spectra of the pristine and the dehydrated phase of **4** show peak bands at 513 and 503 nm, respectively, which indicates that **4** may be used as an attractive material to alter green light to dark red.

A bright blue-green emission can be seen with naked eyes when **5** is irradiated by a UV lamp with an excitation of either 254 or 365 nm. As shown in Figure 14, the emission profile of **5** is very narrow (fwhm of 52 nm) with a peak band at 454 nm and a shoulder peak at 473 nm. Like the framework of **1**, luminescent properties of **5** are also retained if **5** is annealed at 200 or 250 °C, under an air atmosphere for 2 h. The emission of **5** may be originated from a intraligand $\pi-\pi^*$ transition of **L** anion because Na_2L would also give off a bright-blue emission with a peak band at 452 nm and a narrow profile (fwhm of 42 nm).[2c,d,4] However, the excitation spectrum of **5** is broader than that of Na_2L. The excitation spectrum of **5** shows a peak band at 288 nm, which is about 124 nm blue-shifted from that of Na_2L (peak band at 412 nm). The fwhm ranges from 265 to 427 nm. The lifetimes of pristine **5** and those previously annealed at 200 and 250 °C are only 0.82(2) ns ($\lambda_{ex,em}$ = 320,456 nm), 1.1(1) ($\lambda_{ex,em}$ = 370,458 nm), and 0.92(5) ns ($\lambda_{ex,em}$ = 365,-450 nm), respectively, which are obviously shorter than those of **1**. A bright emission, a broad excitation spectrum, a high thermal stability, a short lifetime, and a low solubility make **5** an attractive candidate to protect UV radiation, as well as to transfer UV together with purple light into blue-green light.

Conclusion

In summary, hydrothermal syntheses, crystal structures, and properties (including magnetism, thermal stability, and luminescence) of five new coordination polymers containing fluorescent whitener have been described. Both **1** and **2** possess a novel organic−inorganic hybrid layer composed of binuclear [Cd_2] SBUs (for **1**) or a mono-cobalt node (for **2**), 4,4′-bipy, and an **L** anion. **3** features a pcu-like 3D cationic framework with the inclusion of **L** anions. The structure of **4** can be viewed because the [Mn(4,4′-bipyH)$_2$-(H_2O)$_2$]$^{4+}$ cationic fragment is sandwiched by **L** anions into a sandwichlike hybrid layer. **5** exhibits a 3D honeycomb-like structure, with each nanotube encapsulating two parallel **L** anionic chains. The thermal stabilities of frameworks and fluorescent properties for **1**, **4**, and **5** make them attractive luminescent materials. Preliminary results show that the blue emission of 4,4′-bis(2-sulfonatostiryl)biphenyl can be quenched or altered into bright blue-green, green, and dark-red luminescence by combining them with metal-organic frameworks. Furthermore, luminescent lifetimes can also be adjusted from 0.82 to 39 ns. Future investigation will focus on introducing fluorescent whitener into lanthanide−organic frameworks to assemble a series of new rare-earth materials with intriguing luminescent properties.

Acknowledgment. This research was supported by grants from the State Key Laboratory of Structure Chemistry, the Fujian Institute of Research on the Structure of Matter, the Chinese Academy of Sciences (CAS), the National Ministry of Science and Technology of China (Grants 2006CB932900 and 2007CB815301), the National Science Foundation of China (Grants 20333070, 20673118, and 90406024), the Science Foundation of CAS and Fujian Province for research funding support (Grants KJCX2-YW-M05, 2005HZ01-1, 2007J0171, 2006J0014, and 2006F3132).

Supporting Information Available: X-ray crystallographic data in CIF format for **1**−**5**; more structural figures and luminescent plots of **1**, **4**, and **5**. This material is available free of charge via the Internet at http://pubs.acs.org.

IC700597K